Characteristics and Mechanism of the 10–20-Day Oscillation of Spring Rainfall over Southern China

WEIJUAN PAN

State Key Laboratory of Numerical Modeling for Atmospheric Sciences and Geophysical Fluid Dynamics (LASG), Institute of Atmospheric Physics, Chinese Academy of Sciences, Beijing, and Guangdong Climate Center, Meteorological Administration of Guangdong Province, Guangzhou, China

JIANGYU MAO AND GUOXIONG WU

State Key Laboratory of Numerical Modeling for Atmospheric Sciences and Geophysical Fluid Dynamics (LASG), Institute of Atmospheric Physics, Chinese Academy of Sciences, Beijing, China

(Manuscript received 21 August 2012, in final form 30 December 2012)

ABSTRACT

The intraseasonal oscillations (ISOs) of southern China spring rainfall (SCSR) are examined based on daily rain gauge rainfall data and NCEP/Department of Energy Reanalysis 2 (NCEP-2) products for the period 1980–2008. The objective of this study is to reveal the structure and propagation of the dominant ISO of SCSR as well as its driving mechanisms, thereby gaining an understanding of the causes of extreme wet and dry SCSR.

The EOF analysis and power spectrum analysis show that the 10–20-day oscillation is a predominant ISO of SCSR in most years. Composite analyses and wave-activity propagation diagnosis demonstrate that the 10–20-day oscillation of SCSR is characterized by an alternate occurrence of a huge anomalous anticyclone (cyclone) encircling the Tibetan Plateau in the lower troposphere, with anomalous low-level northeasterly (southwesterly) winds prevailing over southern China, producing lower-tropospheric divergence (convergence). In the middle and upper troposphere, the oscillation appears as a southeastward propagating coherent wave train made up of a series of anomalous cyclones and anticyclones, which are aligned in a northwest–southeast direction. This whole wave train also drifts eastward, with strong upper-tropospheric convergence (divergence) alternately superimposed over the lower-tropospheric divergence (convergence) within and south of the Yangtze basin, resulting in deficient (excessive) rainfall in southern China. The thermal structure of the 10–20-day ISO of SCSR and its association with the mechanical–thermal forcing of the Tibetan Plateau are also explored.

1. Introduction

Since Madden and Julian (1971, 1972) used spectral analysis to discover a 40–50-day eastward-propagating oscillation in the tropics, there has been much interest in the characteristics and mechanisms (Goswami 2005; Waliser 2005, 2006) of intraseasonal oscillations (ISOs). Many studies have shown that ISOs also exist in extratropical regions (Krishnamurti and Bhalme 1976; Ghil and Mo 1991a,b), with different characteristics from tropical oscillations in terms of periodicity and propagation. ISOs have been found to be responsible for variability of the monsoon regime within the annual cycle, significantly influencing local weather and climate (Mao and Chan 2005; Zhou and Chan 2005; Miura et al. 2007). In eastern China, the major rainy season is in summer (June–August) when the monsoonal southwesterlies prevail. Huang et al. (2008) investigated climatological characteristics of the ISO in precipitation over China and suggested that the ISO rainfall amplitudes begin to strengthen in April and weaken in November. An ISO of either 20–30 days (Zhang et al. 2003) or 15–35 days (Mao and Wu 2006) of the summer circulation system over East Asia is associated with the dominant fluctuations in the persistent heavy rainfall over the Yangtze basin, particularly over the lower Yangtze basin for the period from May to August (Yang 2009). Yang et al. (2010) identified two dominant intraseasonal

Corresponding author address: Dr. Guoxiong Wu, State Key Laboratory of Numerical Modeling for Atmospheric Sciences and Geophysical Fluid Dynamics (LASG), Institute of Atmospheric Physics, Chinese Academy of Sciences, P.O. Box 9804, Beijing 100029, China.
E-mail: gxwu@lasg.iap.ac.cn

DOI: 10.1175/JCLI-D-12-00618.1

variations over the lower Yangtze basin during boreal summer (May–August), with spectral peaks occurring around 15 days (the biweekly mode) and 24 days (the 21–30-day mode), which have comparable intensities. Together they account for more than 57% of the total intraseasonal variance, with each mode exhibiting baroclinic structure over the lower Yangtze basin in the extreme phases. However, these two modes differ in genesis and evolution.

Another significant rainy season, the premonsoon, occurs in spring over southern China south of 30°N before the East Asian summer monsoon onset. The precipitation in March and April accounts for one-quarter to one-third of the annual total amount near the mountainous border between Guangdong and Fujian provinces in southern China (LinHo et al. 2008). Similar to the mei-yu period, synoptic-scale fronts frequently occur as a dominant system over southern China, with a strong low-level southwesterly jet near the southeastern coastal region, producing heavy rainfall. Some mesoscale convective systems associated with cold or warm fronts are also observed to be triggered by topography such as the Nan Ling Mountains (LinHo et al. 2008), leading to enhanced precipitation. As the southern China spring rainfall (SCSR) episode is the earliest period of rain after the dry winter in eastern China and directly affects regional agricultural and economic activities, several studies have investigated its formation mechanism from a climate-mean perspective. Tian and Yasunari (1998) suggested that the low-level southwesterly jet associated with seasonal warming in spring is responsible for the formation of the SCSR event, with the time-lag effect in seasonal warming arising from the land–sea thermal contrast between the Indochina Peninsula and the western North Pacific east of the Philippines. However, Wan and Wu (2007) emphasized the primary role of the Tibetan Plateau (TP), with the southwesterly jet resulting from both mechanical and thermal forcing by the TP.

From a planetary-scale perspective, LinHo et al. (2008) linked the onset of SCSR to the seasonal transition of global circulation from boreal winter to spring in East Asia. They suggested that in February the reduced thermal contrast between ocean and land leads to a weakening of the Asian winter monsoon as well as suppressed convection over Australia and the western Pacific Maritime Continent due to the passage of the dry phase of a Madden–Julian oscillation (MJO) event. It is obvious that the SCSR onset involves a series of adjustments of atmospheric circulation systems in both the tropics and midlatitudes.

As SCSR involves an interaction between tropical flow from warm oceans and cold air from midlatitudes, the frontal movements may become slow or even stagnant, leading to persistent rain for several days, and forming active and break sequences in terms of the intensity and duration of rainfall during an individual spring. Such an intraseasonal variability can even be seen in the evolution of climatological SCSR, as was shown by LinHo et al. (2008). SCSR starts around mid-March and the rainfall intensity exhibits several strong and weak periods, indicating a distinct intraseasonal oscillation during spring. However, this variability on intraseasonal time scales has not been documented.

Mao et al. (2010) found that the characteristic period of the predominant intraseasonal oscillation in summer Yangtze rainfall is 20–50 days, and such a 20–50-day oscillation arises in response to intraseasonal variations in the western North Pacific subtropical high, which in turn are modulated by a Rossby wave–like coupled circulation–convection system that propagates northward or northwestward from the equatorial western Pacific. Does a similar situation occur in SCSR? What are the dominant intraseasonal modes that control SCSR activity? In addition to the influence of tropical systems such as the subtropical high, what is the impact of the midlatitude systems on intraseasonal SCSR variability? The objective of this study is to investigate the intraseasonal variability of SCSR in terms of its structure and propagation as well as the mechanism responsible for this variability, in order to understand the causes for the extremes in SCSR.

Section 2 describes the data and methods used in this study. The dominant periodicities of the SCSR ISO are identified in section 3, and the structure and temporal evolution of the 10–20-day ISO are described in section 4. The mechanism responsible for the 10–20-day ISO is investigated in section 5. Finally, a summary and discussion are given in section 6.

2. Data and methods

a. Data

Daily rain gauge precipitation data for 178 observational stations in southern China (defined here as east of 105°E, between 18° and 32°N) for the spring period (March–May) from 1980 to 2008 were provided by the National Meteorological Information Center, China Meteorological Administration (CMA), and were used to produce the climate mean SCSR as shown in Fig. 1a.

Daily atmospheric circulation data were extracted from the National Centers for Environmental Prediction (NCEP)–Department of Energy (DOE) Reanalysis

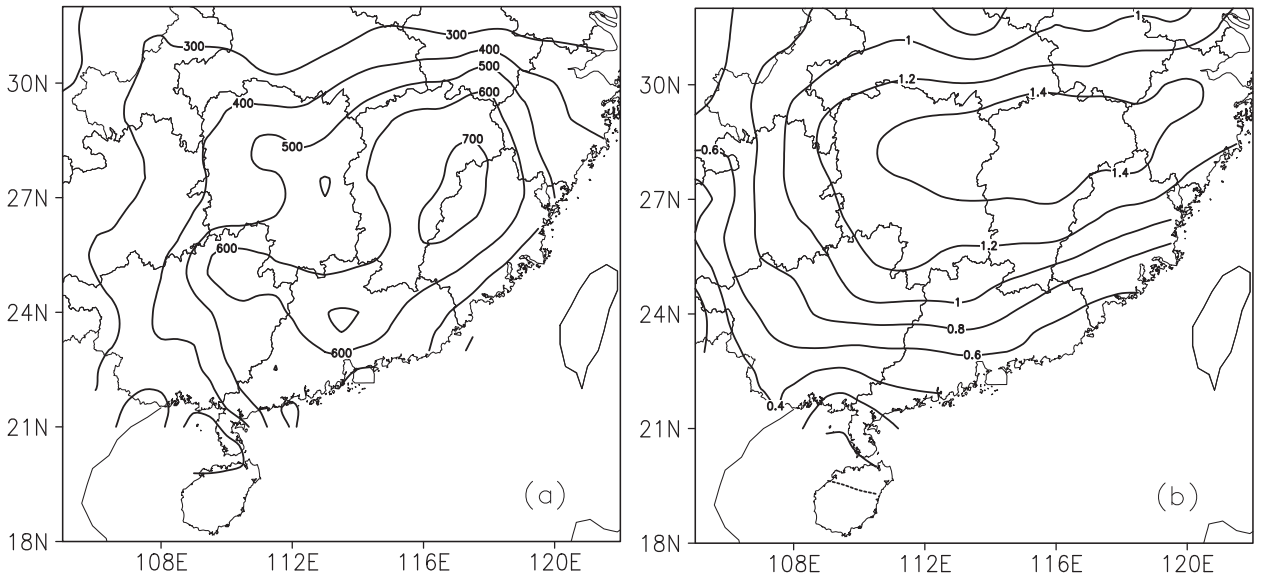

FIG. 1. (a) Spatial distribution of the climatological spring (March–May) precipitation (mm) over southern China for the period 1980–2008. (b) Spatial pattern of the first EOF mode (EOF1) for daily spring precipitation anomalies over southern China.

2 (NCEP-2) from 1980 to 2008 (Kanamitsu et al. 2002), including wind, geopotential height, and temperature, with a horizontal resolution of 2.5° latitude × 2.5° longitude. Also used are daily surface sensible heat fluxes and winds at 10 m, with a T62 Gaussian grid of 192 × 94 points over the whole globe.

b. Methods

According to Mao et al. (2010), the choice and calculation of a reference time series that represents the evolution of spring rainfall over southern China is very important for identifying the dominant ISO component. Therefore we apply the same technique as Mao et al. (2010) and Yang et al. (2010) to spring rainfall time series for each station before employing an empirical orthogonal function (EOF) analysis. First, a 5-day running mean is calculated to remove synoptic fluctuations, and then the climatological daily means for the period March–May are removed from each 5-day running mean time series to produce a daily anomaly time series. Here the climatological daily means are derived from the 5-day running mean time series from 1980 to 2008 for each station. EOF analysis is thus applied to the daily rainfall anomaly time series in southern China for the period March–May from 1980 to 2008. Because the principal component (PC) of an EOF mode can show how the spatial pattern oscillates over time, the corresponding PC of the leading mode (Fig. 1b) that represents the coherent variation of SCSR is selected as the reference time series.

To identify the dominant periodicity, power spectrum analysis (Gilman et al. 1963), which is one of the most common methods of spectral analysis, is applied to the reference time series during each spring. The mean power spectrum is then obtained by taking the average of individual power spectra for 29 spring seasons from 1980 to 2008 so as to obtain the common periodicity characteristics. The statistical significance of the power spectrum is tested based on the method of Gilman et al. (1963) for a red-noise process.

Compared to Fourier harmonic analysis and wavelet analysis, the Lanczos bandpass filter (Duchon 1979) possesses the advantage in terms of significantly reducing the Gibbs oscillation, and has become a commonly used filter in ISO research (e.g., Kikuchi et al. 2012). The Lanczos filter is thus applied in this study to the reference time series of the first principal component (PC1) of the leading EOF mode (as discussed below) to extract the ISO components. Similarly, the corresponding atmospheric ISO signals are extracted from other meteorological fields such as air temperature, geopotential height, and winds. Composite analyses are carried out for the filtered variables to examine the spatial structure and temporal evolution of the ISO, with the statistical significance of composite fields being estimated based on a Student's *t* test.

To estimate the possible routes for the propagation of the ISO, we calculate the phase-independent wave-activity flux **W** formulated by Takaya and Nakamura (2001). In a sphere coordinate, **W** is expressed as follows:

$$\mathbf{W}=\frac{p\cos\phi}{2|\mathbf{U}|}\begin{pmatrix}\dfrac{U}{a^2\cos^2\phi}\left[\left(\dfrac{\partial\psi'}{\partial\lambda}\right)^2-\psi'\dfrac{\partial^2\psi'}{\partial\lambda^2}\right]+\dfrac{V}{a^2\cos\phi}\left[\dfrac{\partial\psi'}{\partial\lambda}\dfrac{\partial\psi'}{\partial\phi}-\psi'\dfrac{\partial^2\psi'}{\partial\lambda\partial\phi}\right]\\ \dfrac{U}{a^2\cos\phi}\left[\dfrac{\partial\psi'}{\partial\lambda}\dfrac{\partial\psi'}{\partial\phi}-\psi'\dfrac{\partial^2\psi'}{\partial\lambda\partial\phi}\right]+\dfrac{V}{a^2}\left[\left(\dfrac{\partial\psi'}{\partial\phi}\right)^2-\psi'\dfrac{\partial^2\psi'}{\partial\phi^2}\right]\\ \dfrac{f_0^2}{N^2}\left\{\dfrac{U}{a\cos\phi}\left[\dfrac{\partial\psi'}{\partial\lambda}\dfrac{\partial\psi'}{\partial z}-\psi'\dfrac{\partial^2\psi'}{\partial\lambda\partial z}\right]+\dfrac{V}{a}\left[\dfrac{\partial\psi'}{\partial\phi}\dfrac{\partial\psi'}{\partial z}-\psi'\dfrac{\partial^2\psi'}{\partial\phi\partial z}\right]\right\}\end{pmatrix}+\mathbf{C}_U M, \quad (1)$$

where ψ' is the streamfunction, (U, V) are zonal and meridional components of the basic flow, (λ, ϕ) are respectively longitude and latitude, a is Earth's radius, p = pressure/1000 hPa, f_0 is the Coriolis parameter, and N is the buoyancy frequency. The wave-activity (angular) pseudo-momentum M is defined as

$$M=\frac{p}{2}\left(\frac{q'^2}{2|\nabla_H Q|}+\frac{e}{|\mathbf{U}|-C_p}\right)\cos\phi, \quad (2)$$

where q' and Q are the potential vorticity of the wave and basic flow, respectively; e is wave energy; ∇_H is a horizontal Hamilton operator; C_p is the phase speed of migratory perturbation in the direction of the basic flow $\mathbf{U}$; and $\mathbf{C}_U$ represents the phase propagation vector in the direction of $\mathbf{U}$ (i.e., $\mathbf{C}_U = C_p\mathbf{U}/|\mathbf{U}|$). For a zonally uniform basic state and when C_p vanishes, (1) becomes the same as the stationary "wave activity flux" defined by Plumb (1985). In this study, C_p is calculated in exactly the same manner as in Takaya and Nakamura (2001), as follows: First, over the whole oscillation period and on a day of different phases, the correlation coefficients of the 10–20-day filtered 200-hPa geopotential height time series between a particular grid point and other grid points with a lag of −24 h are calculated. Then the correlation coefficients are calculated in the same manner but with a lag of +24 h. Next the phase propagation is estimated by tracing the maximum positive correlation center on the one-point correlation maps thus constructed from the negative to positive lag. Finally, the local value of C_p for that grid point is determined as the projection of this phase propagation onto the direction of the local basic flow $\mathbf{U}$.

Because such a phase-independent wave-activity flux $\mathbf{W}$ is parallel to the local three-dimensional group velocity of a wave packet in a weakly varying zonal basic flow [i.e., $\mathbf{W} = \mathbf{C}_g M$, in which M represents the wave-activity (angular) pseudo-momentum], the wave-packet flux $\mathbf{W}$ can depict the wave-packet propagation very well. Thus, it can be used as a diagnostic tool for illustrating the propagation property of the ISO. In the present study, we only compute the horizontal components of the wave-activity flux $\mathbf{W}$ in the upper troposphere to show the horizontal propagation characteristics of the ISO.

3. Spatiotemporal variability of SCSR

a. SCSR spatial pattern

The climatological spring precipitation exceeds 300 mm over the entire southern China region (Fig. 1a). Note that the maximum rainfall (exceeding 600 mm) mostly occurs in the southeastern areas near the coast, with two centers in excess of 700 mm around the Nanling Mountains and the Wuyi Mountains. Wan and Wu (2008) suggested that these rainfall centers may be due to orographic effects that align the axes of the SCSR rainfall belt with those of the mountains.

The EOF analysis is applied to the SCSR dataset described in section 2. The first four leading EOF modes account for 19.6%, 12.8%, 7.8%, and 4.9%, respectively, of the total variance. Each of these modes is separated from the subsequent mode based on the test of statistical significance proposed by North et al. (1982). EOF1 shows a monopole pattern (Fig. 1b) with positive rainfall anomalies covering the entire southern China; this pattern captures the spatial coherence of the SCSR variability. Since the time-varying amplitude of this pattern is reflected by its corresponding PC1 time series for each spring, PC1 is chosen as the reference time series to identify the dominant intraseasonal signals of SCSR.

Figure 2 shows examples of the temporal evolutions of PC1 and the area-averaged rainfall over southern China (18°–32°N, 105°–120°E) for several selected years. Similar variations are found between the two time series for each spring. Several cycles with different amplitudes are observed in each spring, indicating an intraseasonal fluctuation of SCSR. The intraseasonal fluctuations also exist in the climatological SCSR (LinHo et al. 2008), but this feature is more evident for an individual spring (Fig. 2), as seen also in Fig. 2 of Wan and Wu (2007).

b. Identifying the dominant ISO of SCSR

A power spectrum analysis is applied to detect the distinct periods of the PC1 time series of the SCSR for

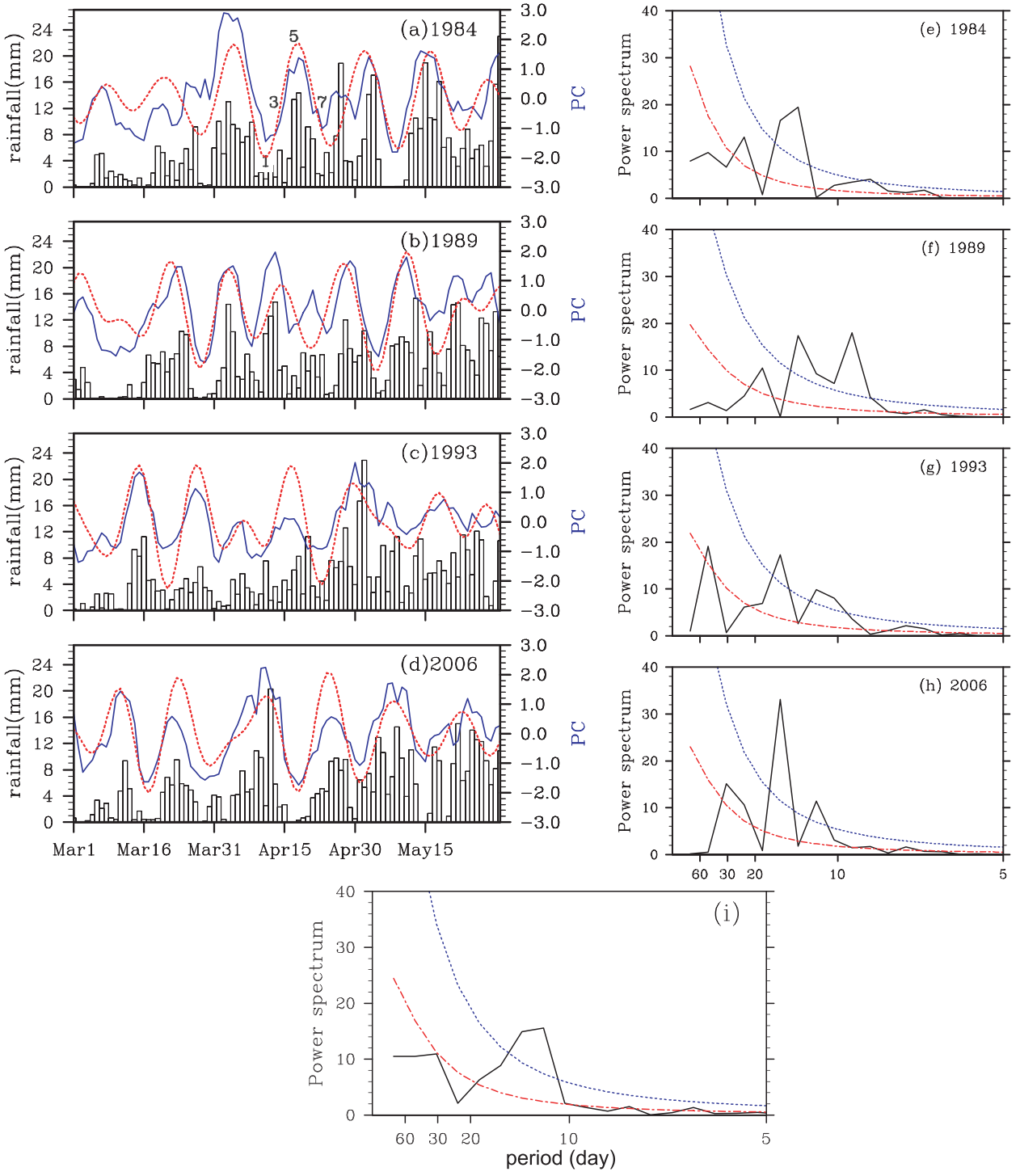

FIG. 2. Time series of daily rainfall (histogram; mm day^{-1}) averaged over southern China (18°–32°N, 105°–120°E), the corresponding unfiltered PC1 (blue solid curve), and the 10–20-day filtered PC1 (red dotted curve) for the typical years of (a) 1984, (b) 1989, (c) 1993, and (d) 2006. (e)–(h) The corresponding power spectrum of the unfiltered PC1 (black curve), together with the Markov red noise spectrum (red dot-dashed curve) and a posterior 95% confidence level (blue dotted curve) for the selected years and (i) the 29-yr average from 1980 to 2008. The numbers 1, 3, 5, and 7 in (a) indicate the phase of the 10–20-day oscillation.

each spring from 1980 to 2008. The power spectra for four individual years are presented as typical examples in Figs. 2a–h. The characteristics of the temporal evolution of daily rainfall averaged over southern China for the selected years (as shown in Figs. 2a–d) is in general captured by the PC1 time series of the SCSR and well depicted by the corresponding 10–20-day filtered PC1. The power spectrum analysis presented in Figs. 2e–h indicates that the 10–20-day band is a significant prominent oscillation period (significant at the 95% confidence level). To identify further the ISO period common to most of the springs, the 29-yr averaged power spectrum is also calculated, and the result (Fig. 2i) again proves that the 10–20-day band is statistically significant.

The focus of the present study is therefore on the 10–20-day ISO of SCSR, with this intraseasonal component extracted from the time series of a particular variable by using the Lanczos filter. The 10–20-day SCSR oscillation in each spring appears as several positive and negative cycles with different amplitudes, as shown in Figs. 2a–d.

4. Structure and evolution of the 10–20-day oscillation of SCSR

To reveal the structure and evolution of the 10–20-day SCSR oscillation, phase compositing of several meteorological variables is performed. The 10–20-day signals in atmospheric circulation in terms of air temperature, geopotential height, and winds at different pressure levels are also extracted by Lanczos filter. Following Mao et al. (2010), the selection of a strong ISO case is based on the 10–20-day filtered PC1 time series shown in Fig. 2. A strong ISO cycle is defined as one including both a wet and a dry period, with the peak amplitude of each period greater than a threshold of one standard deviation. Consequently, 46 strong ISO cycles are selected from 1980 to 2008. Each cycle is further divided into eight phases (see Fig. 2a). Phase 1 represents the minimum value denoting the dry period, while phase 5 is the maximum value corresponding to the wet period. Phases 3 and 7 denote the transition periods. Phases 2, 4, 6, and 8 occur at the time when the oscillation reaches half of its maximum or minimum value. The dynamic structure and evolution of the 10–20-day SCSR oscillation are subsequently examined in terms of tropospheric flow patterns.

a. Low-level circulation

Figure 3 shows the composite evolution of the 10–20-day filtered 850-hPa stream field and divergence during an ISO cycle. In the driest phase (phase 1; Fig. 3a), a significant semiclosed anomalous anticyclone is observed east of the TP, with strong divergence centered on the southeastern foothills of the TP. An anomalous northeasterly on the southeastern side of the anticyclone prevails over southern China. Such a divergent environment is not favorable for local rainfall. This semiclosed anticyclone seems to be the eastern part of a huge ''open'' anticyclone that encircles the TP. In contrast, an apparent convergence zone is located over the northwestern TP between the southwesterly in the south and northwesterly in the north. Associated with this strong convergence is an anomalous westerly flow around 45°N. A significant anomalous easterly flow is also present north of this westerly flow, forming a weak anomalous cyclone over the northern Eurasian continent. The cyclone to the north and the anticyclone encircling the TP thus form an asymmetric dipole with the divergence pole located to the southeast of the TP and the convergence pole to its northwest.

With the weak cyclone in the north and the associated convergence migrating southward, the huge anticyclone surrounding the TP weakens significantly (Fig. 3b), while the semiclosed anticyclone leaves the TP and moves southeastward into the western North Pacific with decreasing intensity. As a consequence, the original strong divergence center is weakened and moves southward to the coastal area of southern China. Note that the northeasterly flow over southern China is replaced by southwesterly flow. Subsequently, both the anomalous southeasterly flow northeast of the TP and the northwesterly flow northwest of the TP strengthen. By phase 3 (Fig. 3c), the southwesterly and southeasterly flows converge along the Yangtze Basin. Both anomalous southerlies from the South China Sea and westerlies south of the TP continue to strengthen, forming a huge cyclone surrounding the TP (Fig. 3d). Because of the strengthening of anomalous southwesterlies southeast of the TP, the convergence zone extends southward significantly, and it intensifies in such a way that southern China is under the influence of anomalous southwesterlies, leading to greater rainfall in the wettest phase (phase 5; Fig. 3e). Subsequently, as the semienclosed cyclone leaves southern China and propagates eastward as a closed smaller-scale system, the anomalous southwesterlies and the upstream westerly flow south of the TP weaken steadily. Anomalous northwesterlies north of the TP and northeasterlies over northern China become active, and a new anticyclone is generated on the eastern TP. It intensifies and propagates gradually southeastward, resulting in divergent conditions around the Yangtze Basin (Figs. 3f,g), thus showing opposite patterns in both divergence and winds to those in phases 2 and 3. This anticyclone together with the divergence continues to propagate southeastward. By phase 8, southern China is dominated by strong northeasterlies again (Fig. 3h) and is located immediately south of the divergence zone, which favors the development of dry conditions.

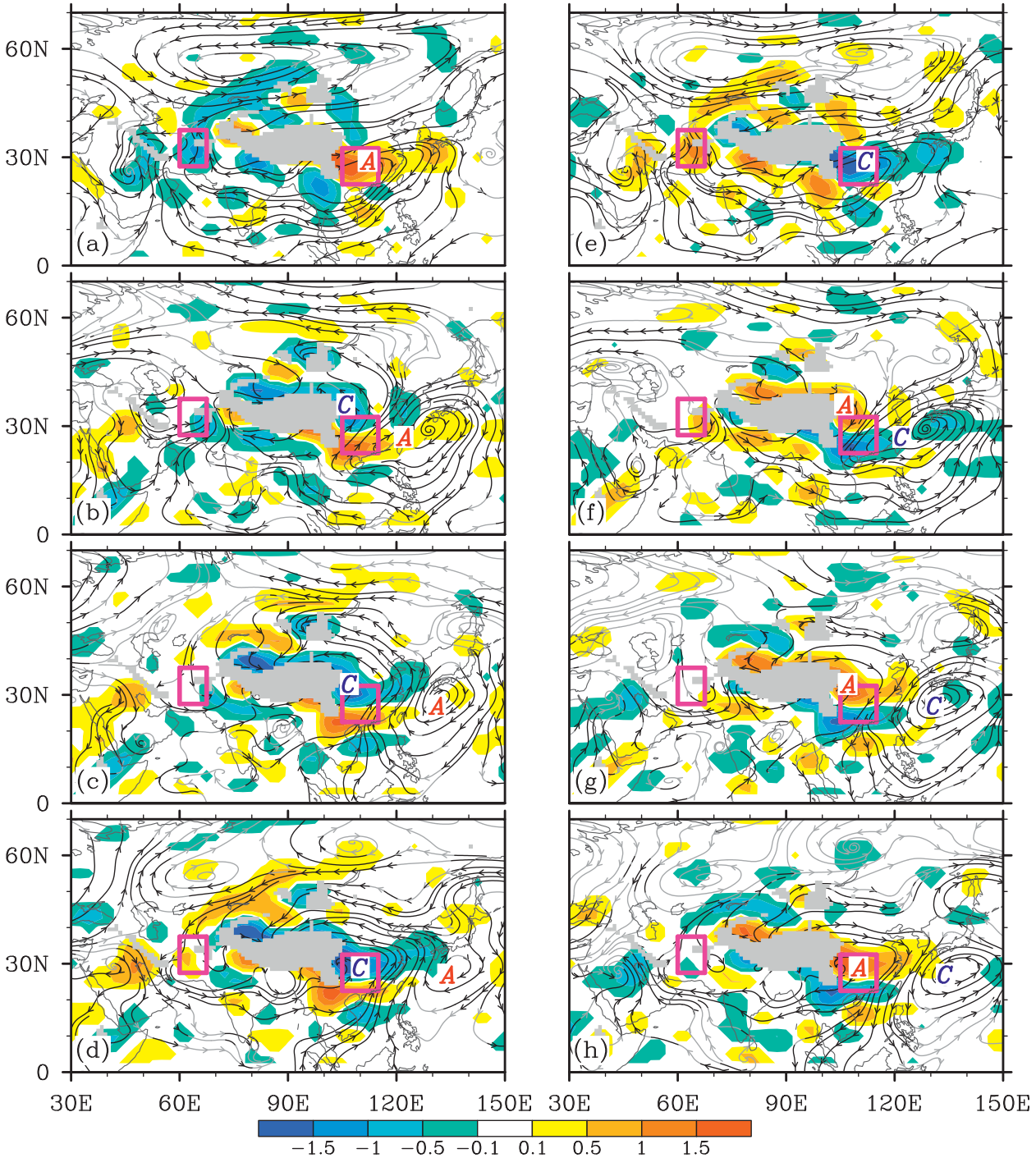

FIG. 3. Composite evolution of the 10–20-day filtered 850-hPa streamline (dark streamline indicates where at least one wind component is statistically significant at the 95% confidence level) and divergence (shading, 10^{-6} s^{-1}; only shown if statistically significant at the 95% confidence level) during an ISO cycle, for (a)–(h) phases 1–8, respectively. The Tibetan Plateau with terrain above 1500 m is shaded gray. The rectangle to the west of the TP (27.5°–37.5°N, 60°–67.5°E) and the rectangle to the east of the TP (22.5°–32.5°N, 105°–115°E) indicate the locations of the two divergence poles of the SDMI. The letters A and C denote the anticyclone and cyclone centers, respectively.

The phases described above demonstrate that the 10–20-day oscillation of SCSR is characterized by an alternate occurrence of a huge anomalous anticyclone (cyclone) encircling the TP in the lower troposphere, with an anomalous low-level northeasterly (southwesterly) prevailing over southern China. This forms lower-tropospheric divergence (convergence) within and to the south of the Yangtze Basin, resulting in deficient (excessive) rainfall in southern China.

During phase 5 (Fig. 3e), the distribution of the 10–20-day filtered 850-hPa stream field is quite similar to the wintertime stationary dipole mode pattern of lower atmospheric circulation surrounding the TP (Wang et al. 2008). This dipole mode is forced mainly by the TP forcing in winter, and is characterized by cyclonic (anticyclonic) circulation to the south (north) of the TP, accompanied by a convergent pole on the east of the TP and a divergent pole on its west. Consequently, to the east of the TP the cold air moves southward along the northern anticyclone circulation and meets the wet and moist southerly along the southern cyclone circulation over southern China, forming the SCSR. The in-phase (out-of-phase) configuration between the aforementioned dipole mode and the 10–20-day filtered 850-hPa stream field at the wet (dry) phase suggests that the dipole mode is enhanced (weakened) at the wet (dry) phase, resulting in excessive (deficit) rainfall in southern China.

Since the pattern and strength of the near-surface circulation around the TP depends to a great extent on the thermal forcing of the TP associated with surface sensible heating (Wu et al. 1997, 2007), the enhancing and weakening of the cyclonic circulation encircling the TP at the wet and dry phases should be associated with the enhancing and weakening of the TP thermal forcing. Figure 4 shows the composite evolution of the 10–20-day filtered 10-m streamlines and surface sensible heat flux. During the driest phase (Fig. 4a), negative surface sensible heating anomalies over the TP correspond to anomalous divergent winds blowing downslope and toward the surrounding areas, accompanied by anticyclonic circulation encircling the TP at 850 hPa (Fig. 3a), and associated with a dominant anomalous southwesterly over most of eastern China and an anomalous northeasterly over the southern coastal region and South China Sea (SCS). An east–west-oriented band of surface divergence is located in southern China in association with the local anticyclonic circulation at 850 hPa (Fig. 3a). During this phase, a significant positive heating anomaly occurs to the north of the TP (Figs. 4a,b). It extends southward in such a manner that the northern TP also becomes a positive heating anomaly region (Figs. 4c,d), with surrounding air converging toward the TP due to the sensible heat-driven air pump (Wu et al. 2007). When positive sensible heating anomalies completely cover the TP at phase 5, anomalous cyclonic circulation encircles the entire TP at 850 hPa (Fig. 3e) and the strongest surface convergence occurs over southern China: the wettest phase is reached (Fig. 4e). Subsequent phases (Figs. 4f–h) take up opposite situations to those in phases 2–4. The above analyses demonstrate that the evolution of the 10–20-day ISO is associated with the polarity cycle of the wintertime TP dipole mode, which is modulated by the thermal status of the TP in the spring season.

b. Upper-level circulation

The composite evolution of the 10–20-day filtered 200-hPa circulation, divergence, and horizontal component of flux wave activity **W** is shown in Fig. 5. During the driest phase (phase 1; Fig. 5a), a significant coherent wave train is present in the upper troposphere. An anomalous elongated anticyclone, accompanied by strong divergence, is situated to the northwest of the TP. Enclosed anomalous cyclonic, anticyclonic, and cyclonic centers are located alternately over the Ural Mountains, Pakistan, and the eastern coast of India. Although each flow pattern is elongated in a relatively narrow band in a northeast–southwest direction, the entire wave train pattern is oriented northwest–southeast. There is another anomalous cyclone centered over Japan, associated with an anticyclone over the South China Sea. The most significant convergence occurs over eastern China, which corresponds to strong lower-tropospheric divergence (Fig. 3a).

Subsequently, the wave train propagates mainly southeastward and eastward, and the divergence–anticyclone zone splits into two distinct centers during phases 2–4, with one located west of the TP and the other located east of the TP (Figs. 5b–d). Note that the range and intensity of the divergence associated with the eastern center increase steadily, and reach their maximum values in the wettest phase (Fig. 5e). At this time, southern China is southwest of the enhanced eastern anticyclonic circulation, and the local strong upper-layer divergence is coordinated with strong convergence in the low level (Fig. 3e), which favors local air ascent. Afterward, this divergence–anticyclone system weakens and moves into the western North Pacific (Figs. 5f–h), with anomalous convergence again developing west of the TP and migrating eastward. A similar wave train also exists at 500 hPa (not shown).

Since in a weakly dissipative atmosphere and at the almost-plane wave limit the phase-independent flux (**W**) of the wave activity (angular) pseudo-momentum (M) is parallel to the local three-dimensional group velocity $\mathbf{C}_g$ (Takaya and Nakamura 2001), by plotting the flux **W** it is possible to obtain the energy propagation of the ISO. During the driest phase (phase 1; Fig. 5a), wave activity flux propagates eastward from western Europe to the

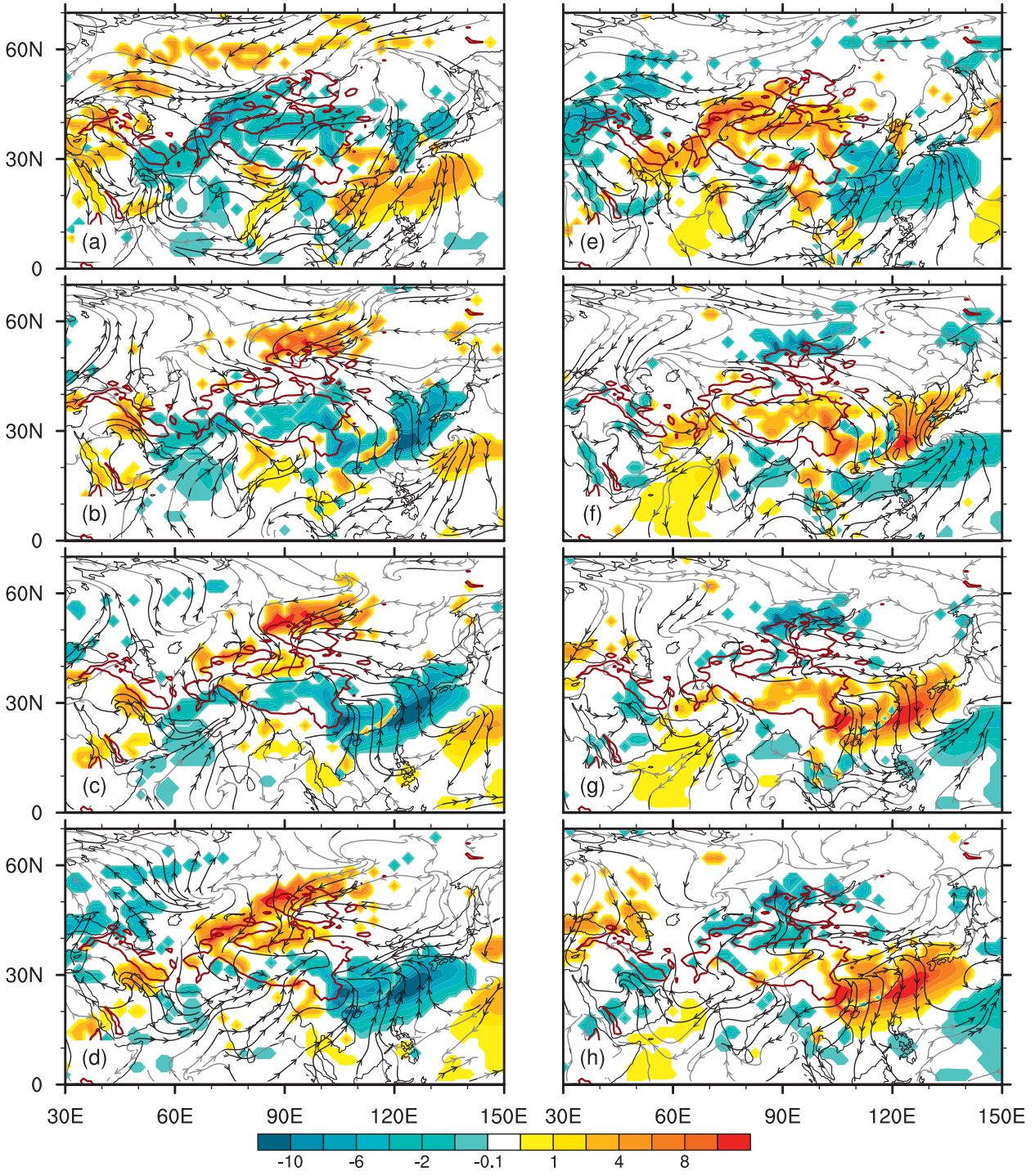

FIG. 4. As in Fig. 3, but for the 10–20-day filtered 10-m streamline and surface sensible heating flux (W m^{-2}, with shading denoting statistical significance at the 95% confidence level). The Tibetan Plateau with terrain above 1500 m is outlined by a solid curve.

Ural Mountains and turns southeastward toward the western TP. Subsequently, the broadened flux sweeps over the TP, with its northern rim propagating from the region near Lake Baikal to Japan and the stronger southern rim encircling the south of the TP toward southern China (Figs. 5b–d). During the wettest phase (phase 5; Fig. 5e), the propagation pattern of wave activity flux is similar to that at the driest phase (phase 1). From phase 6 to phase 8 (Figs. 5f–h) the southeastward flux also propagates in a similar manner. The general

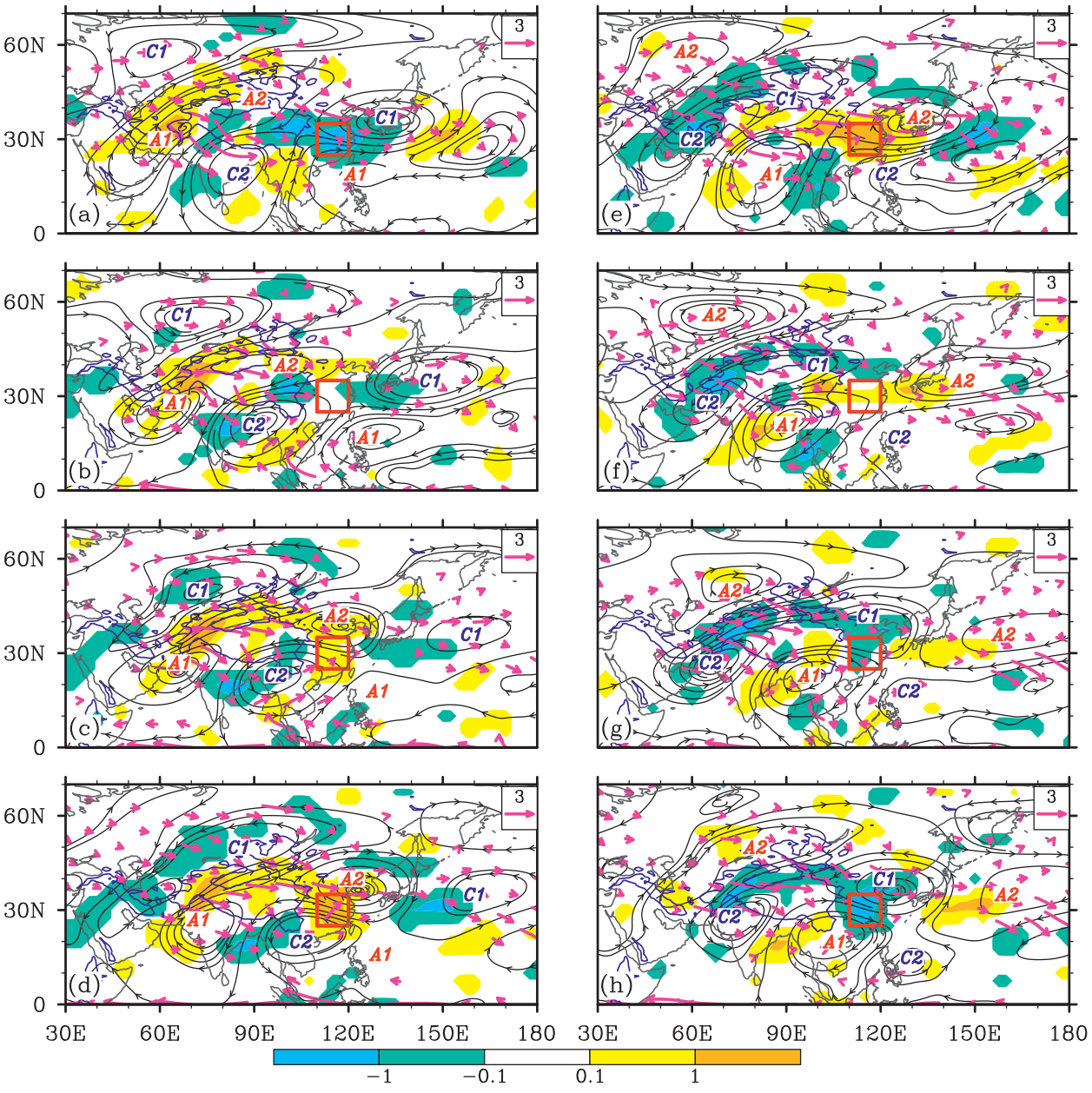

FIG. 5. As in Fig. 3, but for the 10–20-day filtered 200-hPa streamline, divergence (shading, 10^{-6} s^{-1}), and the horizontal component of the wave-activity flux **W** (vector, m^2 s^{-2}). The Tibetan Plateau with terrain above 1500 m is outlined by the solid purple curve. The region bounded by the red rectangle (25°–35°N, 110°–120°E) is used in defining the DIVI.

prevailing southeastward orientation of the **W** flux is in good coordination with the wave train of the 10–20-day stream field at 200 hPa (Fig. 5), indicating that the latter is a manifestation of the 10–20-day ISO energy propagation.

The propagation of the 10–20-day ISO circulation can be viewed from the following alternative perspective. At phase 1 a north–south-oriented cyclone–anticyclone (C1–A1) pair is located over central Asia (Fig. 5a). As the pair propagates east-southeastward, the orientation axis gradually tilts from northeast to southwest (Figs. 5b–d). During the passage of the pair over the TP, the northern cyclonic pole to the north of the TP propagates faster than the southern anticyclonic pole to the south of the TP (Figs. 5d–g). After the pair crosses the TP, its axis becomes northeast–southwest oriented, with strong convergence in between (Fig. 5h). The circulation then moves back to phase 1, with the northern cyclone located over Japan and the southern anticyclone over the

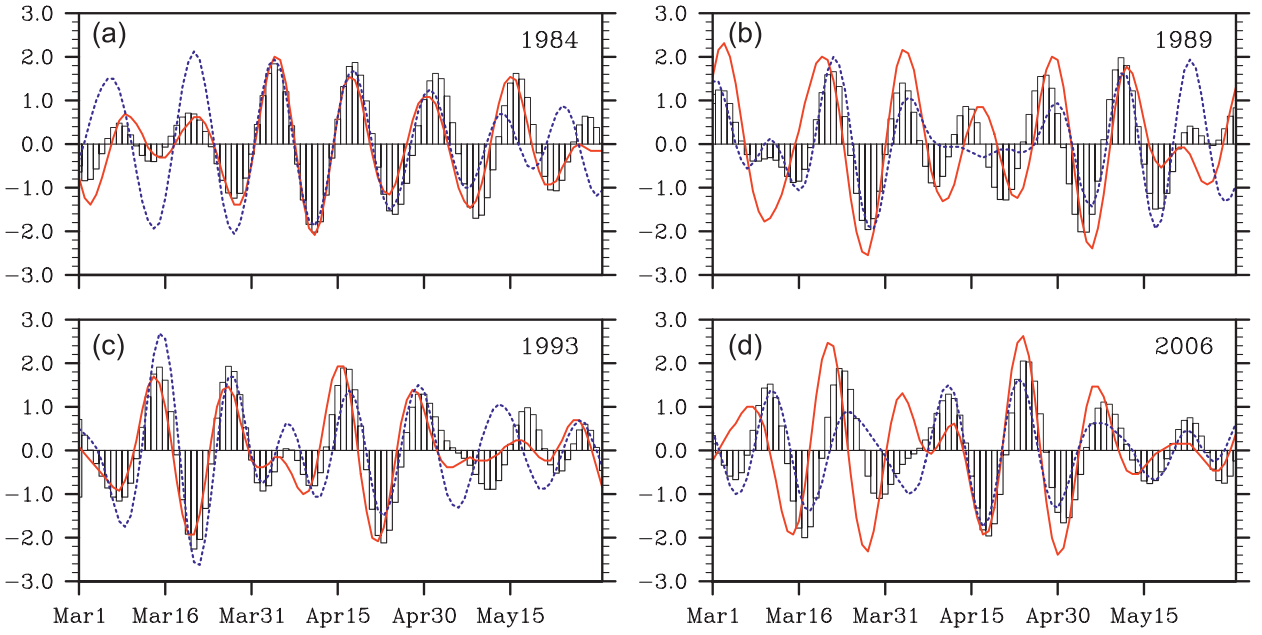

FIG. 6. (a)–(d) Evolution of the 10–20-day filtered time series of PC1 (histograms), the lower tropospheric SDMI (dotted line), and the upper tropospheric DIVI (solid red line) for selected years (shown in the upper right of each panel).

Philippines, and with strong convergence just above southern China corresponding to the driest phase. Thus, the propagation of the C1–A1 system from central Asia to East Asia takes a period of one 10–20-day ISO cycle. At this point another new C1–A1 pair appears over northwest Asia ready to follow the same path as the previous pair, which continues to propagate into the western Pacific. The wave evolution and the formation of the wettest phase follow a similar process but with opposite polarity. As presented in Fig. 5e, a north–south-oriented anticyclone–cyclone pair (A2–C2) is located over central Asia. It then propagates east-southeastward with its northern component A2 moving faster than the southern component C2 (Figs. 5a–c, e–h). When this pair has passed over the TP, its orientation axis assumes a northeast–southwest tilt (Fig. 5d). By phase 5 (Fig. 5e), the anticyclone A2 is over Japan and the cyclone C2 is over the northern Philippines, and strong divergence is located just above southern China, contributing to the local development of air ascent and a persistent SCSR.

Note that the significant divergence (convergence) or cyclone (anticyclone) centers mostly exist around the TP, implying that thermal and mechanical forcing by the TP may modulate the wave train pattern during its propagation. This issue requires further exploration.

c. *Vertical coupling*

The above analysis shows that the evolution of the 10–20-day ISO of SCSR is accompanied by southeastward propagation of a wave train in the middle and upper troposphere, and by a polarity transition of the dipole mode pattern in the lower troposphere. Considering the location of the maximum center of convergence or divergence over eastern China at 200 hPa (Figs. 5a,e), a divergence index (DIVI) is defined as the area-averaged divergence over eastern China (25°–35°N, 110°–120°E, as indicated by a box in Fig. 5) to represent the dynamical pumping effect of the upper-tropospheric circulation. In the lower troposphere, the divergence or convergence on the east of the TP is opposite to that on the west of the TP during the extreme dry or wet phases (Figs. 3a,e); thus, a spring dipole mode index (SDMI) for measuring the TP forcing is defined as the difference in the area-averaged divergence between the key regions to the west and east of the TP (as indicated by the boxes in Fig. 3).

Figure 6 displays the time series of 10–20-day filtered SDMI, DIVI, and PC1 for several typical springs. The 10–20-day ISO index exhibits a distinct in-phase variation with the SDMI, indicating an important role of the TP forcing in modulating the intraseasonal fluctuations of SCSR. The 10–20-day ISO index also evolves in phase with the DIVI, suggesting that the upper-tropospheric dynamical pumping effect in association with the DIVI is indeed important for regulating the 10–20-day ISO of SCSR. The in-phase relationship between the upper-level DIVI and lower-level SDMI represents a close coupling in the vertical, and such a coupling may determine the formation and evolution of the 10–20-day ISO of SCSR.

5. Baroclinicity of the 10–20-day oscillation of SCSR

To explore further the mechanism responsible for the generation and propagation of the 10–20-day ISO, we present pressure–longitude and pressure–latitude cross sections (Figs. 7 and 8) of the filtered geopotential height, air temperature, and winds.

In the driest phase (Fig. 7a), the evident baroclinicity can be identified clearly in the middle and upper troposphere, with a negative temperature center and descending air located west of the negative geopotential height center. There are significant negative temperature anomalies in a band extending from the lower to upper troposphere, with this anomaly pattern tilting westward with increasing height, accompanied by strong descending motion from the upper troposphere to below 700 hPa, indicating that the upper-level cold air has already intruded into eastern China. On the other side, positive temperature anomalies accompanied by westerlies and weak ascending motion exist west of the geopotential height ridge, which is over the western TP. As the positive temperature anomaly moves eastward across the TP in association with the increasing surface sensible heating over the TP (Figs. 4b–d), ascending motions develop over eastern China (Figs. 7b–d), with descending cold air helping the western warm air to uplift, converting available potential energy into kinetic energy. Note the remarkable positive temperature anomalies extending upward to the upper troposphere and westward of the positive height anomalies. When a maximum positive temperature anomaly appears around 200 hPa, with the lower temperature anomaly center and ascending motion both reaching their strongest state, SCSR reaches its wettest phase (Fig. 7e). Afterward cold air crosses the TP and accumulates in the east so that descending motion gradually controls eastern China (Figs. 7f,g), which is unfavorable for SCSR, and the ISO moves back to its driest phase, completing one cycle.

The northward tilting with increasing height of the negative temperature anomaly zone is present from the lower troposphere to around 200 hPa in the driest phase (Fig. 8a), accompanied by strong northerlies and descending motion along the surfaces of pseudo-equivalent potential temperature, indicating that anomalous cold air dominates southern China, with its surface forefront reaching the southern SCS. Significant divergence exists in the lower troposphere over southern China coupled with evident convergence in the middle and upper troposphere. Another negative temperature anomaly in the middle and lower troposphere is located north of 60°N. There is a distinct positive temperature anomaly belt between the two negative anomalies. As the northern negative temperature anomaly subsequently migrates southward (Figs. 8b–d), the warmer air is forced to ascend over southern China, which favors energy conversion from available potential into kinetic energy. When the anomalous cold air intrudes into southern China, the strongest ascending motion occurs, leading to heavy SCSR in the wettest phase (Fig. 8e). Subsequently anomalous cold air completely dominates the lower and middle troposphere over southern China. This suggests that baroclinicity associated with energy conversion is another dominant mechanism for the generation and propagation of the 10–20-day ISO of SCSR.

6. Summary and discussion

Southern China spring rainfall (SCSR) usually undergoes several active and break sequences in terms of the intensity and duration of rainfall during an individual spring. Such intraseasonal oscillations of SCSR are examined based on rain gauge rainfall data and NCEP-2 reanalysis products for the period 1980–2008. The objective of this study is to investigate the structure and propagation of the dominant ISO of SCSR as well as the driving mechanisms, thereby gaining an understanding of the causes of the extreme wet and dry SCSR.

EOF analysis was applied to SCSR data to identify its spatiotemporal variability. The first leading mode (EOF1) captures the spatial coherence of the intraseasonal variability in SCSR, with the corresponding principal component (PC1) for each spring exhibiting evident ISOs. The PC1 was thus used as the reference time series to isolate the dominant intraseasonal signals of SCSR. Spectral analysis of the SCSR PC1 series shows a predominant oscillation of SCSR with a characteristic period of 10–20 days in most years, although interannual differences exist in significant periodicities. The 10–20-day filtered PC1 time series was thus defined as the ISO index of SCSR.

Composite analyses demonstrate that the 10–20-day oscillation of SCSR is characterized by an alternate occurrence of a huge anomalous anticyclone (cyclone) encircling the TP in the lower troposphere, with anomalous low-level northeasterlies (southwesterlies) prevailing over southern China, forming lower-tropospheric divergence (convergence) within and south of the Yangtze basin and corresponding to deficient (excessive) rainfall in southern China. In the middle and upper troposphere the oscillation appears as an eastward and southeastward propagating coherent wave train made up of a series of anomalous cyclones and anticyclones, which are aligned in a northwest–southeast direction. The phase-independent wave-activity flux **W** of the 10–20-day ISO is also oriented southeastward and is in good coordination with the wave train, implying the southeastward energy propagation of

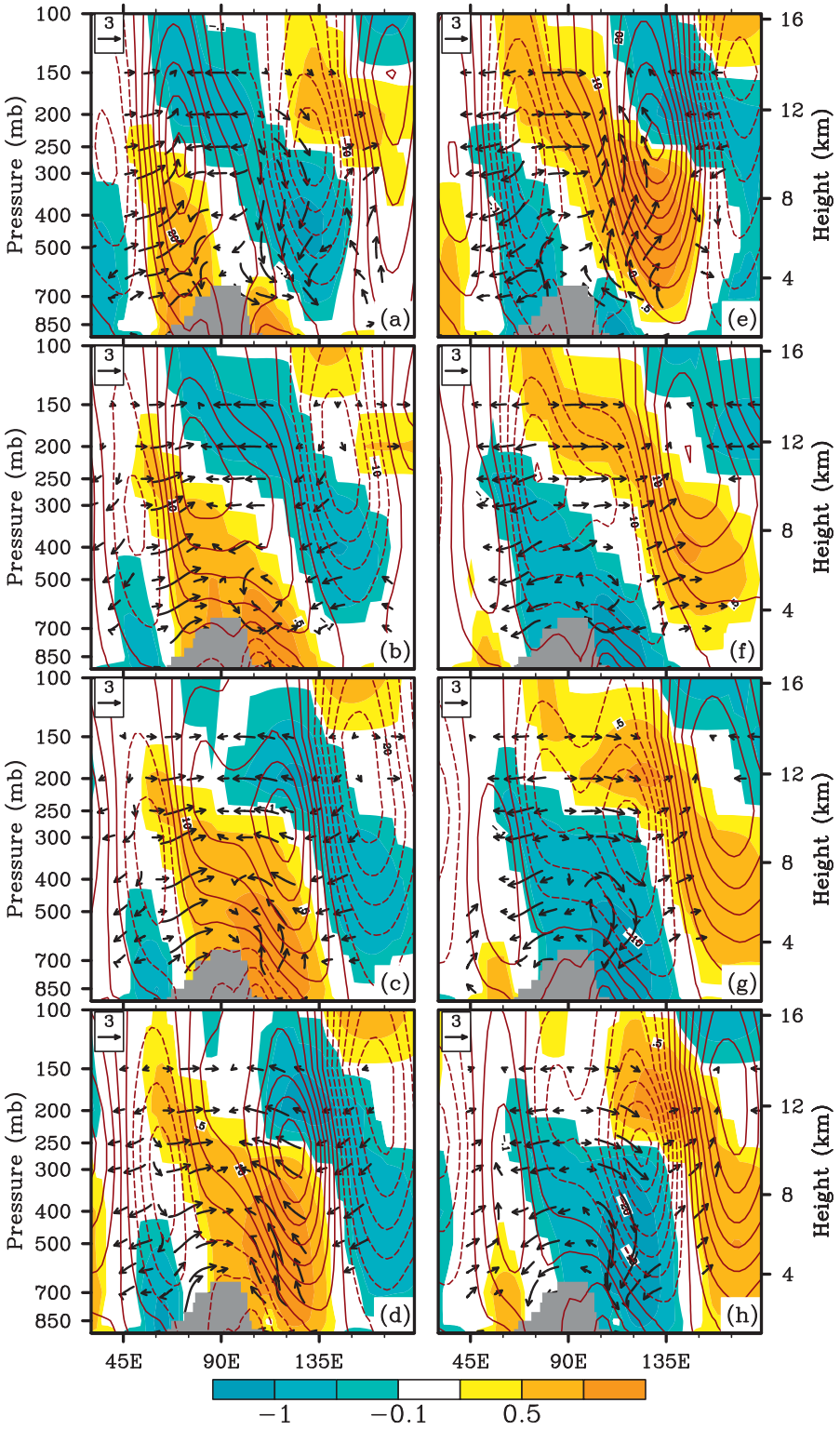

FIG. 7. The (30°–40°N) average pressure–longitude cross sections of composite 10–20-day filtered airflow (vectors, u in m s^{-1}, and vertical velocity in $-200 \times \omega$ Pa s^{-1}), geopotential height (contours, interval is 5 gpm), and air temperature (shading, K) during an ISO cycle, for phases (a)–(h) 1–8, respectively. Only those values of geopotential height, temperature, and wind (at least one component) that are statistically significant at the 95% confidence level are shown. The Tibetan Plateau is shaded gray.

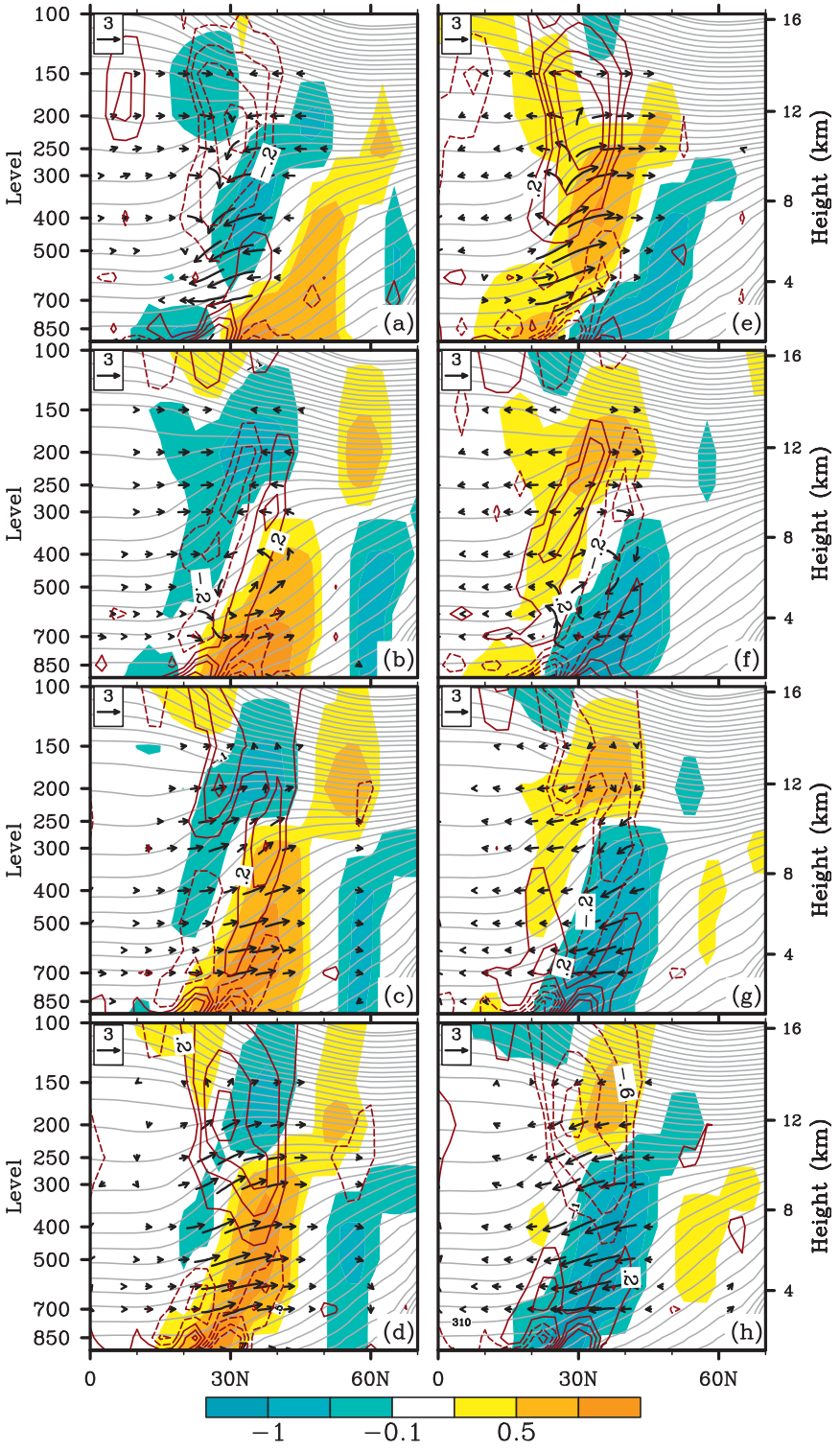

FIG. 8. As in Fig. 7, but for the region 105°–120°E; and divergence (red contours, 10^{-6} s^{-1}) and unfiltered pseudo-equivalent potential temperature (gray contours, K) replacing geopotential height and air temperature.

the ISO. Thus strong upper-tropospheric convergence and divergence occur alternately over eastern China.

The in-phase relationship between the 10–20-day ISO of SCSR and the spring dipole mode index (SDMI) indicates an important role of the TP forcing in modulating such an ISO. The 10–20-day ISO index is also in phase with the upper-layer divergence (DIVI), suggesting that the upper-tropospheric dynamical pumping effect is also important for regulating the 10–20-day ISO of SCSR as well. The in-phase relationship of DIVI at 200 hPa with SDMI at 850 hPa represents a close coupling in the vertical, and such a coupling may determine the formation and evolution of the 10–20-day ISO of SCSR.

The anomalously cold zone tilting both northward and westward with increasing height is present from the lower troposphere to around 200 hPa in the driest phase. Baroclinicity is evident in the free troposphere, with the negative temperature center being located west and north of the negative geopotential height center. As anomalously cold air subsequently migrates southeastward, the warmer air is forced to ascend over southern China, which favors baroclinic energy conversion from available potential energy into kinetic energy. When anomalous cold air intrudes into southern China, the strongest ascending motion takes place, leading to heavy SCSR in the wettest phase. This suggests that baroclinicity is another dominant mechanism for the generation and propagation of the 10–20-day ISO of SCSR.

In addition to the 10–20-day period, the 20–30-day period is also significant in some years (e.g., Yang et al. 2010). Which oscillation characteristics and formation mechanisms are common to the two ISO modes and which are different, and what determines the different periodicity? These are unknown but important questions for understanding SCSR and its variability, and need to be explored further.

Notice that during the dry (wet) phase, the surface divergent (convergent) streamline over the TP, as shown in Fig. 4a (Fig. 4e), implies a predominant local downslope (upslope) flow as a consequence of the TP surface cooling (heating). This then contributes to the development of a huge anomalous anticyclone (cyclone) encircling the TP at a lower level (850 hPa), as demonstrated in Fig. 3a (Fig. 3e), presenting a dynamically consistent inherent configuration. However, it remains unclear whether the 10–20-day oscillation is an intrinsic atmospheric motion embedded in the westerly or whether it is forced (regulated) by recharge–discharge of boundary energy on the Tibetan Plateau is still unclear. Notice also that the phase-independent wave-activity flux **W** of the 10–20-day ISO propagates from western Europe to eastern Asia and that divergence of the flux is over Europe, indicating that the energy source is from the west. The southeastward propagation of the flux indicates that the 10–20-day band is an intrinsic and characteristic period of atmospheric circulation, and is regulated by the boundary energy forcing of the Tibetan Plateau. However, it is still unclear why this period is an intrinsic and characteristic period of atmospheric circulation. In any case, further studies are required to better understand the genesis and propagation of such a 10–20-day oscillation.

Acknowledgments. The authors thank the three anonymous reviewers for their constructive suggestions. NCEP–NCAR reanalysis data were obtained from the NOAA-CIRES Climate Diagnostics Center, Boulder, Colorado. This research was jointly supported by the National Basic Research Program of China (Grants 2012CB417203 and 2011CB403505) and NSFC Grants 40975052, 41175059, and 41275088.

REFERENCES

Duchon, C. E., 1979: Lanczos filtering in one and two dimensions. *J. Appl. Meteor.,* **18,** 1016–1022.

Ghil, M., and K. Mo, 1991a: Intraseasonal oscillations in the global atmosphere. Part I: Northern Hemisphere. *J. Atmos. Sci.,* **48,** 752–779.

——, and ——, 1991b: Intraseasonal oscillations in the global atmosphere. Part II: Southern Hemisphere. *J. Atmos. Sci.,* **48,** 780–792.

Gilman, D. L., F. J. Fuglister, and J. M. Mitchell Jr., 1963: On the power spectrum of red noise. *J. Atmos. Sci.,* **20,** 182–184.

Goswami, B. N., 2005: South Asian summer monsoon. *Intraseasonal Variability of the Atmosphere–Ocean Climate System,* W. K. M. Lau and D. E. Waliser, Eds., Springer, 19–62.

Huang, F., S.-N. Huang, and X. Zhang, 2008: Study on the climatological intraseasonal oscillation of Chinese rainfall (in Chinese). *J. Ocean Univ. China,* **38,** 173–177.

Kanamitsu, M., W. Ebisuzaki, J. Woollen, S.-K. Yang, J. J. Hnilo, M. Fiorino, and G. L. Potter, 2002: NCEP–DOE AMIP-II Reanalysis (R-2). *Bull. Amer. Meteor. Soc.,* **83,** 1631–1643.

Kikuchi, K., B. Wang, and Y. Kajikawa, 2012: Bimodal representation of the tropical intraseasonal oscillation. *Climate Dyn.,* **38,** 1989–2000.

Krishnamurti, T. N., and H. N. Bhalme, 1976: Oscillations of a monsoon system. Part I: Observational aspects. *J. Atmos. Sci.,* **33,** 1937–1954.

LinHo, L.-H., X.-L. Huang, and N.-C. Lau, 2008: Winter-to-spring transition in East Asia: A planetary-scale perspective of the south China spring rain onset. *J. Climate,* **21,** 3081–3096.

Madden, R. A., and P. R. Julian, 1971: Detection of a 40–50 day oscillation in the zonal wind in the tropical Pacific. *J. Atmos. Sci.,* **28,** 702–708.

——, and ——, 1972: Description of global-scale circulation cells in the tropics with a 40–50 day period. *J. Atmos. Sci.,* **29,** 1109–1123.

Mao, J.-Y., and J. C. L. Chan, 2005: Intraseasonal variability of the South China Sea summer monsoon. *J. Climate,* **18,** 2388–2402.

——, and G.-X. Wu, 2006: Intraseasonal variations of the Yangtze rainfall and its related atmospheric circulation features during the 1991 summer. *Climate Dyn.,* **27,** 815–830.

——, Z. Sun, and G.-X. Wu, 2010: 20–50-day oscillation of summer Yangtze rainfall in response to intraseasonal variations in the subtropical high over the western North Pacific and South China Sea. *Climate Dyn.,* **34,** 747–761.

Miura, H., M. Satoh, T. Nasuno, A. T. Noda, and K. Oouchi, 2007: A Madden–Julian oscillation event realistically simulated by a global cloud-resolving model. *Science,* **318,** 1763–1765.

North, G. R., T. L. Bell, R. F. Cahalan, and F. J. Moeng, 1982: Sampling errors in the estimation of empirical orthogonal functions. *Mon. Wea. Rev.,* **110,** 699–706.

Plumb, R. A., 1985: On the three-dimensional propagation of stationary waves. *J. Atmos. Sci.,* **42,** 217–229.

Takaya, K., and H. Nakamura, 2001: A formulation of a phase-independent wave-activity flux for stationary and migratory quasigeostrophic eddies on a zonally varying basic flow. *J. Atmos. Sci.,* **58,** 608–627.

Tian, S.-F., and T. Yasunari, 1998: Climatological aspects and mechanism of spring persistent rains over central China. *J. Meteor. Soc. Japan,* **76,** 57–71.

Waliser, D. E., 2005: Predictability and forecasting. *Intraseasonal Variability of the Atmosphere–Ocean Climate System,* W. K. M. Lau and D. E. Waliser, Eds., Springer, 389–424.

——, 2006: Intraseasonal variability. *The Asian Monsoon,* B. Wang, Ed., Springer, 203–258.

Wan, R.-J., and G.-X. Wu, 2007: Mechanism of the spring persistent rains over southeastern China. *Sci. China,* **50D,** 130–144.

——, and ——, 2008: Temporal and spatial distribution of the spring persistent rains over southeastern China (in Chinese). *Acta Meteor. Sin.,* **66,** 310–319.

Wang, T.-M., G.-X. Wu, and R.-J. Wan, 2008: Influence of the mechanical and thermal forcing of Tibetan Plateau on the circulation of the Asian summer monsoon area (in Chinese). *Plateau Meteor.,* **27,** 1–9.

Wu, G.-X., W.-P. Li, and H. Guo, 1997: The Tibetan Plateau's sensible heating air pump and Asia summer monsoon (in Chinese). *The Zhao Jiuzhang Festschrift,* Beijing Science Press, 116–126.

——, and Coauthors, 2007: The influence of mechanical and thermal forcing by the Tibetan Plateau on Asian climate. *J. Hydrometeor.,* **8,** 770–789.

Yang, J., B. Wang, B. Wang, and Q. Bao, 2010: Biweekly and 21–30-day variations of the subtropical summer monsoon rainfall over the lower reach of the Yangtze River basin. *J. Climate,* **23,** 1146–1160.

Yang, Q.-M., 2009: The 20–30-day oscillation of the global circulation and heavy precipitation over the lower reaches of the Yangtze River valley. *Sci. China,* **52D,** 1485–1501.

Zhang, Q.-Y., S.-Y. Tao, and S.-L. Zhang, 2003: The persistent heavy rainfall over the Yangtze River valley and its associations with the circulations over East Asia during summer (in Chinese). *Chin. J. Atmos. Sci.,* **27,** 1018–1030.

Zhou, W., and J. C. L. Chan, 2005: Intraseasonal oscillations and the South China Sea summer monsoon onset. *Int. J. Climatol.,* **25,** 1585–1609.